Measurements of the magnetic dipole moments of the antiproton and the Σ^- hyperon*

B. L. Roberts,† C. R. Cox, M. Eckhause, J. R. Kane, and R. E. Welsh
College of William and Mary, Williamsburg, Virginia 23185

D. A. Jenkins and W. C. Lam
Virginia Polytechnic Institute and State University, Blacksburg, Virginia 24061

P. D. Barnes, R. A. Eisenstein, J. Miller,‡ and R. B. Sutton
Carnegie-Mellon University, Pittsburgh, Pennsylvania 15213

A. R. Kunselman
University of Wyoming, Laramie, Wyoming 82070

R. J. Powers
California Institute of Technology, Pasadena, California 91125

J. D. Fox§
Brookhaven National Laboratory, Upton, New York 11973
(Received 3 April 1975)

The fine-structure splittings in atoms formed by stopping antiprotons in Pb and U and Σ^- hyperons in Pb and Pt have been measured. Since the fine structure is produced through the interaction of the magnetic dipole moment of the $\bar{p}$ or the Σ^- with the Coulomb field of the nucleus, a value for the magnetic moment can be determined from the splitting. The magnetic moment obtained for the $\bar{p}$ was (-2.819 ± 0.056) nuclear magnetons, which agrees well with the CPT prediction of -2.793 nuclear magnetons. The magnetic moment derived for the Σ^- was (-1.48 ± 0.37) nuclear magnetons, which is in agreement with the sign given by simple SU(3) theory, but differs somewhat from the value of -0.9 nuclear magnetons predicted by the theory with no mass breaking.

I. INTRODUCTION

When a negatively charged hadron is captured into a bound state about an atomic nucleus it may cascade toward lower atomic states by Auger and radiative transitions.[1-4] If the orbiting hadron possesses half-integral spin, the atomic states will be split by the fine-structure interaction. x rays emitted during transitions between such states will consist of several components whose energy difference is determined by the fine-structure splitting. Since the fine-structure splitting arises from the interaction between the magnetic dipole moment of the orbiting particle and the Coulomb field of the nucleus, a measure of this splitting constitutes a direct measurement of the magnetic moment of the particle.

In the first part of this experiment, atoms of antiprotonic Pb and U were formed directly by bringing to rest in the target material a secondary $\bar{p}$ beam, produced in the external proton beam of the Brookhaven National Laboratory Alternating Gradient Synchrotron. In the second part, kaons were stopped in targets of Pt, Pb, and U. Σ^- hyperonic atoms were then formed through the process[5]

$$K^- + N \rightarrow \Sigma^- + \pi .$$

Some of the resulting Σ^- hyperons escaped from the nucleus in which they were produced and formed Σ^- atoms with other target nuclei.

We have measured the fine-structure splitting in $\bar{p}$-Pb, $\bar{p}$-U, Σ^--Pt, and Σ^--Pb, the results of which have been reported in earlier letters.[6-9] In this paper we present a detailed description of both the experimental arrangement and the analysis of the data, as well as a more thorough discussion of the results obtained and conclusions to be drawn from them.

II. THEORETICAL CONSIDERATIONS

A. Magnetic moments

The value of the magnetic dipole moment of the antiproton can be predicted with a high degree of certainty. The CPT theorem requires that particle-antiparticle pairs have magnetic moments equal in magnitude and opposite in sign.[10] Since the CPT theorem is known to hold to a very high accuracy,[11] an experimental determination of the magnitude of the $\bar{p}$ magnetic moment and of its sign can therefore be viewed as a test of the experimental and analytical techniques used to determine the Σ^- magnetic moment.

The Σ^- magnetic moment is less clearly theoretically related to previously measured magnetic moments. The moment can be given in terms of the magnetic moments of the other members of the baryon octet by SU(3),[12-14] and in fact a precise measurement of the Σ^- moment would be a useful test of SU(3) theory. Notwithstanding the difficulty of correctly including the strong interactions in the dynamics of the problem,[12] SU(3) theory with no mass breaking predicts[13]

$$\mu(\Xi^-) = \mu(\Sigma^-) = -[\mu(p) + \mu(n)]. \tag{1}$$

Furthermore SU(6), or a model with equal-mass quarks, predicts[14]

$$\frac{\mu(p)}{\mu(n)} = -\tfrac{3}{2}.$$

Thus

$$\mu(\Sigma^-) = -\tfrac{1}{3}\mu(p) = -0.9\mu_N, \tag{2}$$

where $\mu_N = e\hbar/2m_pc$, one nuclear magneton. The possibility that the strange quark has a mass which is different from the isodoublet members has been considered by Rubinstein *et al.*[14]

B. Atomic effects

The magnetic moment of a $\bar{p}$ or Σ^- can be decomposed into two components,[15]

$$\mu = (g_0 + g_1)\mu_H,$$

where g_0 is the Dirac factor (equal to the particle charge, $+1$, -1, or 0) and g_1 is the Pauli or anomalous term. Both components are expressed in units of the appropriate hadron magneton, $\mu_H = e\hbar/2m_Hc$, where m_H is the hadron mass. The fine-structure splitting of an atomic level with principal quantum number n and orbital angular momentum quantum number l is given by[15]

$$\Delta E_{n,l} = (g_0 + 2g_1)\frac{(\alpha Z)^4}{2n^3}\frac{m}{l(l+1)}, \tag{3}$$

where Z is the nuclear charge, m is the reduced mass of the hadron-nucleus system, and α is the fine-structure constant. For $\mu < 0$, the state of larger j is higher in energy. Equation (3) was derived in the Pauli approximation[15] and neglects terms of order $(v/c)^4$ or higher. Since $\bar{v}/c \approx Z\alpha/n$, we can see that for $n = 10$ and $Z = 92$, the most extreme case considered in this work, the contribution of the neglected terms is of the order of 10^{-5} below those considered here.

From the atomic transitions between two fine-structure doublets shown schematically in Fig. 1, several results are apparent. The intensity of the transition from state j_4 to j_1 is negligible because $\Delta j = 2$. If one assumes a statistical population of the levels, the intensity ratio for transitions $a:b:c$ is given[15] by the expression

$$a = \frac{1 + (2j_1+1)/(2j_2+1)}{(2j_3+1)/(2j_4+1) - (2j_1+1)/(2j_2+1)},$$

$$b \equiv 1, \tag{4a}$$

$$c = a\left(\frac{2j_3+1}{2j_4+1}\right) - 1.$$

If we define circular transitions as those between levels with $l = n-1$ and noncircular transitions as those between levels with $l \leq n-2$ for which $\Delta n = -1$, then for circular transitions and the first noncircular transitions ($l = n-2$)

$$\begin{aligned} &\text{Circular:} \quad a = 2n^2 + n - 1, \\ &\qquad\qquad\ c = 2n^2 - n - 1, \\ &\text{Noncircular:} \quad a = 2n^2 - 3n, \\ &\qquad\qquad\ c = 2n^2 - 5n + 2, \end{aligned} \tag{4b}$$

where n is the principal quantum number of the final state. For large n, the contribution of transition b can be neglected and one observes experimentally two lines, a and c, which are separated in energy by an amount δE given by

$$\delta E = \Delta E_{n,l} - \Delta E_{n',l'}, \tag{5}$$

where the appropriate ΔE is given by Eq. (3). Therefore, a measurement of the splitting of the two components a and c yields a direct measurement of the magnitude of the magnetic moment. Since the intensity ratio, $R = a/c$, is not unity, it is also possible to determine the sign of the magnetic moment.

There are several effects whose contributions

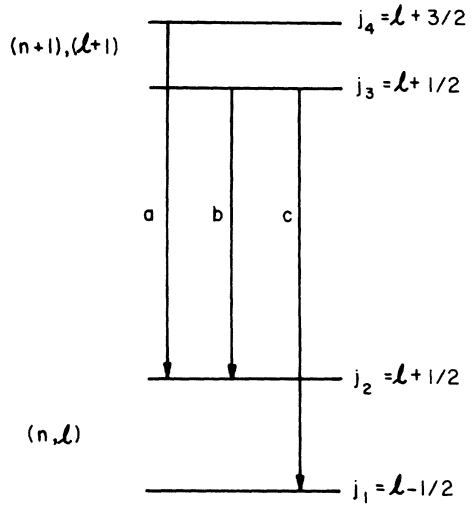

FIG. 1. $E1$ transitions between two fine-structure states.

must be taken into account in an analysis of fine-structure splitting. Noncircular transitions will complicate the observed lineshape. Dynamic quadrupole mixing can change the energy levels given by usual Dirac theory. Changes in the level populations may occur owing to Auger transitions. These will be considered in order.

Figure 2 shows schematically a circular transition labeled γ and the most intense noncircular one α with a competing $\Delta n = -2$ transition β. From Eq. (3) one sees that the splitting of the noncircular transition α is greater than that of the circular one γ. However, the energies of α and γ are not experimentally resolved, and therefore one should include the contribution from α in an analysis for fine-structure splitting. The contribution due to the presence of noncircular transitions can be estimated in two different ways: (1) an estimate based on a cascade calculation, or (2) a direct determination from the experimental data. Only for the analysis of the $\Sigma^-(n=12\rightarrow n=11)$ x ray and of the antiprotonic x rays between high-n levels was the latter possible.

To estimate the contribution of noncircular transitions to the observed $\bar{p}$-Pb and $\bar{p}$-U x-ray lines, a cascade calculation similar to those described by Sapp[16] was performed. Only the first noncircular transition was included in the analysis for fine-structure splitting. The other noncircular transitions were much less intense and would be experimentally resolved in energy from the circular and first noncircular transitions.

For the $\Sigma(12\rightarrow 11)$ transition in Pb, it was possible to estimate experimentally the contribution due to the transition α. The intensity ratio α/β is easily calculated for electric dipole radiation, and an upper limit on $\beta/(\alpha+\gamma)$ can be measured from the experimental data because β and γ are clearly resolved in energy. The intensity ratio $G=\alpha/\gamma$ can be determined from the intensity ratio I, where

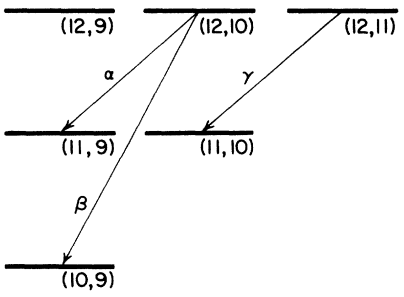

FIG. 2. Schematic diagram of circular and noncircular transitions considered in the analysis of the Σ x-ray data. Levels are labeled by (n,l) values. The fine-structure splittings are not shown.

$$I = \frac{\alpha}{\alpha+\gamma} = \frac{\beta}{\alpha+\gamma}\,\frac{\alpha}{\beta}\,.$$

From the $\Sigma^-(12\rightarrow 11)$ and $\Sigma^-(12\rightarrow 10)$ transitions in Pb we found an upper limit on $\beta/(\alpha+\gamma)$ of 0.07. The intensity ratio α/β calculated for electric dipole radiation is 2.3 for the relevant Σ^- lines in Pb. We then obtain the results

$$I \leq 0.16 \text{ and thus } G \leq 0.19\,.$$

For the $\bar{p}$-U system the effects of dynamic quadrupole mixing must be considered. The Hamiltonian for the hadron-nucleus system is composed of three parts: (1) H_N which operates only on the dynamical variables of the nucleus, (2) H_H which operates only on the variables of the hadron (the hadron-atomic Hamiltonian), and (3) H_{HN} which represents the hadron-nucleus interaction and which operates on both sets of variables. The total Hamiltonian of the system is given by

$$\mathcal{H} = H_N + H_H + H_{HN}\,.$$

In principle, the term H_{HN} will mix nuclear and hadronic states. For our work, the most important example of an interaction which mixes the nuclear and hadronic states is dynamic quadrupole mixing. This mixing is important for deformed nuclei and therefore must be included in any analysis of the U-hadronic x-ray spectra. This dynamic $E2$ effect was first treated theoretically by Wilets[17] and Jacobsohn[18] for muonic atoms, and a more complete treatment has been carried out by Chen.[19] When the off-diagonal matrix elements of the quadrupole interaction reach a value comparable in magnitude with the excitation energy of the first excited nuclear state, then the contribution of the dynamic $E2$ interaction becomes important and a shift in energy occurs. Shifts in K^-, $\bar{p}$, and Σ^- energy levels in ^{238}U have been calculated by Ara and Chen,[20] and observed by Cheng *et al.*,[21] as well as in the present work. An equal shift of both components of a fine-structure doublet does not affect a measurement of the magnetic moment. However, the $E2$ interaction mixes the states such that the new sets of eigenstates are linear combinations of the states coupled by the interaction and j is no longer a good quantum number.

Calculations were made for only the first excited state of ^{238}U using the formalism given by Chen.[19] These calculations showed that the $\bar{p}$-U fine-structure doublet lines ($n=11\rightarrow 10$, $l=10\rightarrow 9$) were shifted equally to within 20 eV, a difference which is far less than the experimental precision of approximately 80 eV. The calculated shifts agreed

well with the more complete calculation of Ara and Chen.[20] For the $n=10$, $l=9$ level of $\bar{p}$-U the interaction energy is approximately 6 keV compared to 44 keV for the excitation of the first excited state of the ^{238}U nucleus. This interaction was sufficient to induce a shift in the energy levels but the resulting hyperfine structure was negligible. For muonic ^{238}U where the interaction energy is of the order of 100 keV, the hyperfine structure has been observed experimentally by McKee for the K, L, and M muonic transitions.[22]

If the hadron were to undergo the $M1$ Auger transition ($\Delta n=0$, $\Delta l=0$, $\Delta j=-1$) from the upper to the lower state in a fine-structure doublet, the statistical population of the fine-structure levels would be destroyed and the simple intensity formulas given by Eq. (4) would no longer be valid. Except for the $\Delta l=0$ transitions, Auger transitions obey the same selection rules as electromagnetic radiation.[23] Thus, the Auger transitions of $\Delta l=-1$ would not affect the statistical population of the atomic levels as given by Eq. (4a). It is thus desirable to calculate the $M1$ Auger rate to see if it is much less than the radiative rates. Following the discussion by Burbidge and de Borde[24] the Auger rate may be calculated in a nonrelativistic approximation. The largest amount of energy available is the fine-structure splitting of 2.97 keV of the $\bar{p}(n=11)$ state in U, which is sufficient to remove an electron from states of $n\geq 4$. Hydrogenic wave functions were employed both for the antiproton and the atomic electron, the latter being assumed to be in the electronic $4s$ state which has the greatest overlap with the $\bar{p}$ at low n. Screening of the $4s$ electron due to inner electrons and the $\bar{p}$ was taken into account by using an effective Z for the electron as described by Slater.[25] The $\bar{p}$ was assumed to be in an $n=11$, $l=10$ state. The number of transitions per second is given by[26]

$$P_A=\left|\frac{1}{\hbar}\int\int \chi_f^*\psi_f^*\frac{e^2}{r_{12}}\chi_i\psi_i\,d\tau_1 d\tau_2\right|^2,$$

where $\chi_{i,f}$ are the initial and final $\bar{p}$ wave functions, and $\psi_{i,f}$ are the initial and final electron wave functions, respectively. The results of this calculation yielded $P_A=9\times10^7$ sec^{-1}, which is much less than the competing radiative rate $P_R=9.6\times10^{16}$ sec^{-1} from the $n=11$, $l=10$ state.

III. EXPERIMENTAL PROCEDURE AND DETAILS

A. Introduction

The data were taken using a secondary beam produced by the slow extracted proton beam of the Brookhaven National Laboratory Alternating Gradient Synchrotron (AGS). Secondary particles ($\pi^-, K^-, \bar{p}$) at 800-MeV/c or 750-MeV/c momentum were brought through an electrostatic separator which permitted selection of a K^- or $\bar{p}$ beam. The stopping particles were detected and identified by means of a scintillation-counter array. The antiprotons or kaons were slowed down in Cu or Fe degrader in combination with graphite or Be and were brought to rest in a high-Z target. Targets of Pt, Pb, and U were employed for the K^--Σ^- experiments and Pb and U for the $\bar{p}$ experiments. The resulting hadronic x rays were observed with a lithium-drifted germanium [Ge(Li)] detector and the corresponding pulse heights were digitized and stored in a multichannel analyzer.

B. Description of beam

The beam design is described in detail elsewhere.[27-30] The slow extracted proton beam from the AGS impinged upon a production target of either Cu or W. The resulting secondary beam particles entered a magnetic lens system at an angle of 10.5° from the forward direction with a solid-angle acceptance of 2.7 msr. The magnetic lens system consisted of six quadrupole and three dipole magnets, with the last dipole and quadrupole being movable so as to produce a momentum recombined or momentum-dispersed beam at the final focus. The momentum slit was set to accept a ± 2% momentum spread centered for the K^- beam on 800 MeV/c and on 750 MeV/c for $\bar{p}$. All of the $\bar{p}$ data described here were taken using the momentum dispersive beam as were kaonic data in natural Pb and depleted U. Natural Pt, Pb, and ^{208}Pb were used as targets in the K^- work done in the recombined beam. These beams were brought to focus on targets placed about 1.7 m downstream of the last quadrupole.

The desired particles (K^- or $\bar{p}$) were selected out of those produced at the production target by the electrostatic separator, with additional requirements imposed by the counter and logic arrangements described below. The K^-/π^- ratio varied between 0.10 to 0.16 depending on the mass slit opening and the $\bar{p}/\pi^-$ ratio was approximately $\frac{1}{75}$.

Production targets 5.08 cm and 7.62 cm in length were employed. For both the $\bar{p}$ and K^- beams, the number of particles per beam burst could be increased by using the larger target; however, this change lessened the beam purity and increased the spot size.

Several degrader arrangements were used but all consisted of Cu or Fe followed by a low-z element such as C or Be. The low-z degrader was placed on the downstream side to minimize multi-

ple scattering, which increases as particles approach low energies. With a 4 g/cm^2-thick stopping target the stop rate was approximately 350 $\bar{p}$ and 2000 K^- per 10^{12} protons incident on the production target. Typical proton intensities were 0.5×10^{12} sec^{-1}.

C. Counter arrangement and electronic logic

Although there existed slight differences between the counter array and electronic logic used to define stopping $\bar{p}$ or K^-, the setups were quite similar. The scintillation-counter arrangement is shown in Fig. 3. Counters 1 through 5 were plastic scintillation counters and C was a Čerenkov counter. In the $\bar{p}$ beam C was a Lucite threshold Čerenkov counter used to reject pions and was placed in anticoincidence with counters 1, 2, 3, and 4. For the K beam, C was a Fitch-type Čerenkov counter[31] used to select kaons in the incident beam and was placed in coincidence with counters 1, 2, 3, and 4.

The Fitch counter consisted of a Lucite radiator viewed by six RCA 8850 photomultiplier tubes arranged symmetrically. Since the Fitch counter is a velocity-selection device, Čerenkov light from an 800-MeV/c K^- escaped from the Lucite to be detected by the photomultipliers, while light from 800-MeV/c pions was totally internally reflected and was not collected. The requirement that two or more of the photomultiplier tubes register pulses coincidentally minimized effects due to beam particles entering the radiator at slightly different angles. A K^- signature of purity > 99% was obtained when a threefold coincidence was required.

Counter 3 was a 10.16 cm×10.16 cm×1.27 cm counter viewed by two photomultiplier tubes which were required to give coincident signals. The outputs from the 10th dynode of each tube were added linearly and this sum was used to impose a dE/dx requirement on the stop signature. Counter 4 was a 0.16-cm-thick 10.16 cm×10.16 cm counter for the momentum-dispersed beam and 12.7 cm×10.2 cm for the momentum-recombined beam.

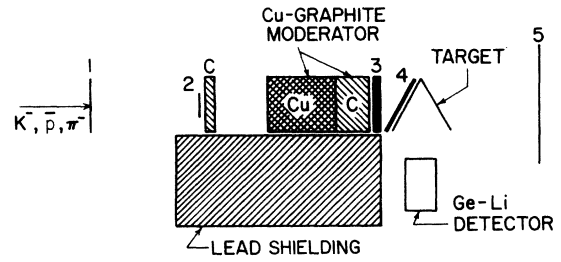

FIG. 3. Target and counter geometry drawn to approximate scale. The Pb shielding was 0.6-m thick in the direction of the beam. Counter 4 was placed immediately upstream of the target.

Counter 5, a 30.5 cm×30.5 cm×0.64 cm scintillator placed 0.5 m behind the x-ray target, was used as a veto counter for differential range curve measurements made in the $\bar{p}$ runs and early K^- runs. Since the use of counter 5 improved the Σ^- x-ray signal-to-noise ratio, it was left in the stop signature for later K^- runs. The use of counter 5 did cause rejection of some true K^- events due to production of prompt pions from nuclear capture. This effect was small, however, since counter 5 was moved downstream so as to subtend less than 1% solid angle at the target during data-taking.

A time-of-flight requirement was placed on the stop signature for the $\bar{p}$ runs by means of a small plastic counter, Z, placed directly after the mass slit (approximately 8 m upstream of the x-ray target). The delay between Z and 1234 was adjusted such that only particles with the transit time characteristic of a 750-MeV/c $\bar{p}$ were accepted. The resulting stop signature for a $\bar{p}$ was then $12\bar{C}3(dE/dx)4Z$. For K^-, the stop signature was $12C3(dE/dx)4\bar{5}$.

D. X-ray detection

During the course of the experiment several Ge(Li) detectors were employed, but all usable data were taken with two 50 cm^3 true coaxial detectors. These exhibited resolutions of 1.10 keV and 0.98 keV full width at half maximum (FWHM) at 292 keV, the energy of the $K^-(9-8)$ transition in Pb. The preamplifiers were both of the cooled FET type and were furnished by the manufacturer as an integral part of the detector system.

The preamplifier signal was fed into a commercial linear amplifier, the output of which was sent directly to the analog to digital converter (ADC) of a 4096 channel multichannel analyzer equipped with a two-point digital stabilizer. The analyzer was interfaced so that the contents of memory could be written on magnetic tape.

The instrumental response of the detector system should generally be Gaussian assuming high charge collection efficiency in the Ge(Li) detector. If radiation damage caused by neutrons occurs in the detector, a low-energy tail will develop on the peaks in the spectrum because of charge trapping in lattice defects created by the neutrons. Only for K^- data taken with the momentum recombined beam was this effect significant. In this case the instrumental shape could be determined using the unbroadened K^- lines and calibration lines from radioactive sources.

E. Fast-slow timing

A "fast-slow" coincidence is formed at some point in the electronic logic in order to ensure that x rays are in time coincidence with the corresponding stopped beam particle. The electronic logic used is shown in Fig. 4. The signal from one of the preamplifier outputs was sent through a fast linear amplifier and then to a timing discriminator. The output signal from the timing discriminator was put in coincidence with a stop signal from the fast logic. The γ timing signal input was approximately 10 nsec wide and the stop signal 60 to 120 nsec wide. This latter width was determined using the characteristic width of the spectrum of the time to amplitude converter (TAC). The delay between the stop and γ signals was adjusted so that a coincident output corresponded to an event in the prompt timing peak of the TAC spectrum. This signal was used to gate the PHA for digitizing and storing the energy signal from the Ge(Li) detector.

F. Energy Calibration and stabilization

In order to determine the energies of the hadronic x rays which were observed, it was necessary to calibrate the detector-analyzer system with radioactive sources whose γ-ray energies fell in the range of interest. Because of count-rate dependence of the instrumental response of the system, it was necessary to calibrate under conditions approximating as closely as possible those under which the data were taken. These conditions were met by placing sources near the detector and increasing the width of the stop pulse to 6 μsec. Any γ ray occurring within this period following a stopped beam particle was stored in the analyzer memory. During all data and calibration runs two γ-ray sources (^{141}Ce at 145.44 keV and ^{137}Cs at 661.635 keV) were placed near the detector. A two-point digital stabilizer continuously monitored and corrected the gain and intercept of the ADC to ensure that these two γ-ray peaks were kept centered in preselected channels in the analyzer. Stabilization corrections were made during the beam-off portion of the AGS pulse cycle by the following method. A "beam-off" gate was used to inhibit the memory "add-1" command of the multichannel analyzer. Any γ ray detected during this beam-off time was digitized but not added to memory. This method permitted the stabilizer to correct changes in gain, but prevented source lines from accumulating in the data. During the beam spill, only γ-ray events in coincidence with stopped beam particles were digitized, and these were added to memory. The stabilization sources were placed sufficiently far from the detector to ensure a low counting rate; almost no accidental coincidences between stabilization γ rays and stopped beam particles occurred. During the calibration runs the stabilization lines accumulated sufficiently slowly so that corrections during any single beam spill were negligible. This method of stabilization is valid so long as the beam rate is kept reasonably steady, as it was during the course of the experiment.

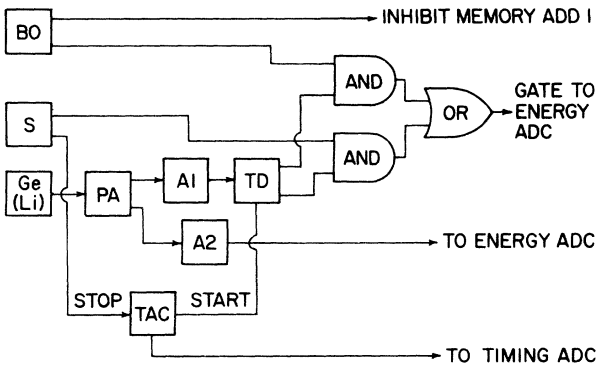

FIG. 4. Fast-slow and gating logic used with the multichannel analyzer. The output of BO was the "beam off" signal and that of S the particle stop signature. PA was the cooled FET preamplifier, $A1$ and $A2$ linear amplifiers (see text), TD the timing discriminator, and TAC was the time to amplitude converter.

The above calibration procedure was not used for the $\bar{p}$ data taken in our earlier runs. A slightly different scheme was employed whereby during calibration runs the system was allowed to stabilize in beam-on as well as beam-off periods, while during the x-ray runs themselves, only for beam-off times. The different stabilization methods used in calibration vs data runs resulted in a zero shift in the calibration spectra which still permitted an accurate gain calibration (eV/channel) but a less accurate absolute energy calibration due to the beam-on beam-off intercept shift. Consequently, although it was straightforward to measure a fine structure splitting from these data, absolute $\bar{p}$ x-ray energies were obtained to less precision.

G. Targets

The x-ray targets used in this work were positioned in a "V" configuration with the detector positioned at the inside of the V. This configuration presented a maximum target thickness to the beam while minimizing the thickness the x rays had to traverse before escaping from the target. For the K^--Σ^- experiments one had to ensure that the target was not so thin as to permit too large a fraction of the produced hyperons to escape. A de-

scription of the targets used is given in Table I.

IV. DATA ANALYSIS

The x-ray data were analyzed using standard least-squares fitting routines. The analysis was carried out on the William and Mary IBM 360/50, the BNL CDC 6600, the CMU UNIVAC 1108, and the VPISU IBM 370/158 computers. For all the x-ray transitions analyzed in this work, the natural (Lorentzian) line width due to the strong interactions was negligible (<10 eV) compared to the instrumental width characteristic of the Ge(Li) detector system. This latter shape was taken to be Gaussian, but was modified when necessary to include a low-energy exponential tail when the response of the detector changed due to charge trapping in lattice defects caused by neutron damage. The specific functional forms used in the least-squares fits are discussed below.

A. Calibration analysis

The calibration lines from radioactive sources and K^- x rays were fitted to a Gaussian function plus an exponential background of the form

$$F(x) = A\exp[-(x-x_0)^2/2\sigma^2] + B_0\exp[\lambda(x-x_0)] = G(x) + B(x), \quad (6)$$

where x_0 was the Gaussian center, σ the FWHM divided by 2.3546, A the amplitude of the Gaussian, B_0 the background height under the peak center, and λ was an exponential constant for the background. In those cases in which a low-energy tail was present, the fitting region was divided into two parts. A parameter ξ was defined such that for $x \leq (x_0 - \xi)$ the function $G(x)$ was replaced by an exponential of the form[32]

$$T(x) = A\exp\{2\xi[x-(x_0-\xi/2)]/2\sigma^2\}, \quad x \leq (x_0-\xi) \quad (7)$$

where the other parameters have the same meaning as in Eq. (6). The functional form was chosen so that both the functions and their derivatives were continuous at the matching point $(x_0 - \xi)$.

The replacement of the Gaussian by an exponential on the low-energy side was necessary only in the last K^--Σ^- data accumulated. For the analysis of the $\Sigma^-(12 \to 11)$ fine-structure components, the adjacent $K^-(9 \to 8)$ was first fitted with the parameter ξ free. Although within statistics the value of ξ obtained agreed with that determined by fitting lines from radioactive sources, the shape used in the Σ^- analysis was taken from the adjacent $K^-(9 \to 8)$ transition because this line was accumulated under conditions identical to that of the $\Sigma^-(12 \to 11)$.

In order to obtain an absolute energy calibration of the Ge(Li)-multichannel analyzer system, the centroids of lines of known energies were used. A least-squares fit was performed with first-, second-, and third-order polynomials. The best fit was determined by using the F test[33] to check the validity of additional terms. Once the best fit representing energy as a function of channel number was determined, the energies of the hadronic x rays could be obtained.

TABLE I. Target Dimensions. The thickness given is the total actual thickness of the target. In cases where several sheets of different sizes were used simultaneously, all are listed. D stands for the momentum dispersive beam and R the momentum recombined one.

Beam	Target material	Length (cm)	Width (cm)	Thickness (g/cm^2)
K^-D	^{197}Au	9.65	9.65	8.3
$\bar{p}$D	Natural Pb	12.7	12.7	5.4
$\bar{p}$D	Depleted U	10.2	12.7	4.5
K^-D	Natural Pb	12.7	12.7	6.8
K^-D	Depleted U	11.1	14.0	1.55
		10.2	14.0	1.53
		8.6	11.4	3.03
K^-R	Natural Pb	12.7	10.2	10.2
K^-R	Natural Pb	12.7	10.2	6.8
K^-R	^{208}Pb	7.6	7.6	7.2
K^-R	Natural Pt	12.7	10.2	6.8

B. Analysis for fine-structure splitting

With the exception of the $\bar{p}(11 \to 10)$ transition in U, the two fine-structure components in a $\bar{p}$ or Σ^- x ray were separated by less than one FWHM, i.e., these lines did not satisfy Rayleigh's criterion for the resolution of two spectral lines.[34] It was necessary to develop a method of analysis for these data which permitted one to determine the separation of the two centroids. These two unresolved components will be referred to as a doublet in the following discussion.

The functional form for a doublet was defined as

$$D(x) = RA_2\exp\{-(x-x_0)^2/2\sigma^2\} + A_2\exp\{-[x-(x_0+\delta)]^2/2\sigma^2\}, \quad (8)$$

in which A_2 was the amplitude of the second component and δ the separation between centers of the two components. In all fits, the widths of the two Gaussians were assumed to be equal, thereby making R [=Amplitude (1)/Amplitude (2)] the ratio of areas as well as the ratio of amplitudes for the doublet members. The statistical ratio a/c as defined by Eq. (4) was used for R, and it was held fixed. Since the noncircular transitions also con-

tributed to the observed line, a second doublet function $D'(x)$ was defined as

$$D'(x) = R'A_2 \exp\{-(x - x'_0)^2/2\sigma^2\} + A_2 \exp\{-[x - (x'_0 + \delta')]^2/2\sigma^2\}, \quad (9)$$

where x'_0 was the different center due to the j dependence of the solution to the Dirac equation, δ' was the splitting of the noncircular doublet as given by Eqs. (3) and (5), and R' was the ratio defined by Eq. (4).

The resulting functional form was

$$F(x) = D(x) + GD'(x) + B(x), \quad (10)$$

with the background term taken to be the same as in Eq. (6). The relative intensity G of the noncircular contribution ($G = \alpha/\gamma$, see Fig. 2) was estimated from either the experimentally determined ratio I, or from a cascade calculation, both of which are discussed in Sec. II. For the $\bar{p}$ data, where such an estimate of G was not possible for the transitions of lower n, G was treated as a free parameter in the least-squares fit, provided that the fit converged. If the fit did not converge, then G was estimated from the cascade program and held fixed. Fits were then performed over a range of values of G, the interval being determined by the range of predictions from the cascade program that were consistent with relative yields of the $\Delta n = -2$ and $\Delta n = -1$ transitions for higher n. It should be noted that the presence of the $D'(x)$ term in the analysis added no more independent parameters because both x'_0 and δ' were related to x_0 and δ through the Dirac equation. In those situations for which it was necessary to include an exponential tail on the low-energy side, each Gaussian was treated separately using the parameter ξ determined from the $K(9 \rightarrow 8)$ transition, as discussed above.

In the $\bar{p}$ transitions for which the separation between the two doublet components was sufficiently large, the separation was treated as a free parameter. The ratio of areas was held fixed as described above. For the higher transitions, the widths of the doublets were also held fixed at the instrumental width obtained as described below. The data were fitted with three different widths: the measured instrumental width, the measured width plus its standard error, and the measured width minus its standard error.

If the separation between the doublet components was less than 40% of one FWHM, it became necessary to hold the separation fixed for a given fit. It was no longer valid to let δ be a free parameter because the error determined from the error matrix reached the same order of magnitude as the value obtained for δ. One thus chose to use the range over which χ^2 changed by one unit as the standard error rather than the value obtained from the error matrix, since the criterion of requiring χ^2 to change by one unit is always valid so long as one can make a parabolic expansion of the χ^2 hypersurface in the region of the χ^2 minimum.[33] One should note that for an error much smaller than the parameter itself, the two methods give the same value for the standard error. For each fit the free parameters included the background amplitude and exponential constant, the center of the first Gaussian (the second center being a fixed distance δ away for each fit) and the amplitude of the second Gaussian (the amplitude of the first Gaussian being determined from RA_2). All widths were assumed equal and held fixed.

A series of fits was made for each fine-structure doublet, with the parameter δ held fixed for each fit. From a fit over a range of δ it was possible to obtain χ^2 as a function of δ, thus enabling one to obtain "most probable" values for δ. Since δ is the difference of the fine-structure splittings for successive n levels, a value for the magnetic moment was thereby obtained. For $n > 10$ the ratio R [$= a/c$, Eq. (4b)], differs from unity by 10% or less, and it was not always possible to obtain a clear indication of the sign of the magnetic moment.

For the $\bar{p}(12 \rightarrow 11)$ and $(11 \rightarrow 10)$ lines in both Pb and U the sign obtained for the magnetic moment was unambiguous. Fits to the Σ^- data were sensitive to the magnitude of the magnetic moment, but the preference for a negative sign was not as pronounced. The value of the magnetic moment was taken to be that at which the χ^2 function reached a minimum and the statistical error was taken to be the interval over which χ^2 changed by one unit.[33]

The instrumental width of the lines used in the series of least-squares fits for the Σ^- data was determined from the following considerations. The $K^-(9 \rightarrow 8)$ x ray observed in Pb is a superposition of two transitions: that between the energy levels $(n = 9, l = 8) \rightarrow (n = 8, l = 7)$ and that for $(9, 7) \rightarrow (8, 6)$ in an intensity ratio of approximately 5. The energies of these two components computed from the Klein-Gordon equation differ by 586 eV which corresponds to approximately 0.5 FWHM for our resolution. The presence in the data of the noncircular transition tends to increase the width as well as shift the energy centroid higher if the two peaks are fitted to a single Gaussian. The $K(9 \rightarrow 8)$ was fitted to a doublet function [see Eq. (8)] over a range of ratios of circular to noncircular intensities, with the relative separation set equal to that predicted by the Klein-Gordon equation, and all other parameters free. The effect of this ratio on the extracted line-width is

displayed in Fig. 5. The cascade program predicted an intensity ratio of 5.2, which results in a width of 7.57 channels. An error of 15% was assigned to the ratio reflecting the precision with which the cascade program predicted the relative yields of the kaonic x rays. This uncertainty in the intensity ratio corresponded to a range of width in channels from 7.50 to 7.65, and agreed with the 7.4 ± 0.3 predicted from radioactive calibration lines. The $K(9 \rightarrow 8)$ transition at 292 keV when fitted to a *single* Gaussian exhibited the same width 8.2 ± 0.3 in the calibration run as it did in the data runs, a width considerably broader than the γ-ray lines at 276 keV (7.02 ± 0.29) and 303 keV (7.71 ± 0.15) from ^{133}Ba. This observation confirmed the conclusion that the broadening in the $K(9 \rightarrow 8)$ line was due to a contribution from the first noncircular transition and not, for example, from pulse pileup in the detector during the beam spill. The instrumental width was taken to be the central value in the range determined from the cascade program, and the error on it to be the quadrature of the errors due to the uncertainty in the circular to noncircular intensity ratio and that due to statistical uncertainty in the least-squares fit with this ratio set equal to its central value.

For some of the $\bar{p}$ data, the instrumental width was obtained from calibration runs as well as from K^- x rays accumulated with a Au target under similar running conditions.

Since the instrumental width was held fixed in generating the χ^2 function vs doublet separation δ, it was necessary to vary the width over the range of its experimental uncertainty and to study its effect on the value extracted for magnetic moment. The precision given for the moment reflects the uncertainties in both the instrumental width and

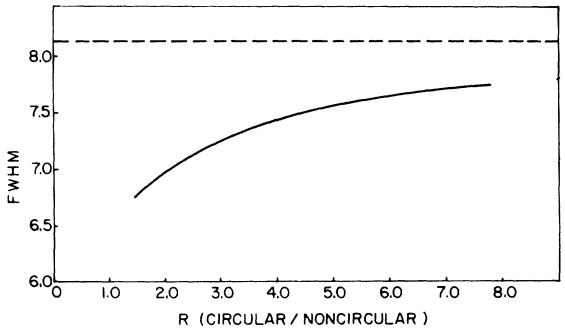

FIG. 5. Instrumental resolution extracted as a function of the ratio of the circular to first noncircular transitions for the $K^-(9 \rightarrow 8)$ transition in Pb. The FWHM is given in channels with one channel corresponding to 148 eV. The dashed line represents the width obtained from a single Gaussian fit to the complex $K^-(9 \rightarrow 8)$ line.

in G, the relative intensity due to the noncircular transitions.

C. Data simulation

In order to test the methods of least-squares fitting used and to study the effect of contributions from inner transitions, simulated data were generated using a computer. The input to the program was the functional form given by Eq. (10), which was then randomized with Gaussian statistics. These simulated data were then analyzed by the same least-squares fitting routine used to fit the actual data. The results obtained from these simulated data exhibited the same sensitivity to G as did the results from the experimental data and added to the confidence which one can have in the analysis program.

V. RESULTS AND CONCLUSIONS

The tabulated masses,[35] $m_p = (938.2592 \pm 0.0052)$ MeV, and $m_{\Sigma^-} = (1197.34 \pm 0.07)$ MeV were used in the computation of the respective moments following Eq. (3). The errors in the values of the magnetic moments associated with the uncertainties in the contributions of noncircular transitions and in the instrumental linewidth were common to the analysis of both $\bar{p}$ and Σ^- data. We shall discuss effects relevant to both analyses before presenting the values obtained. The K^--Σ^- data in U were not used for the Σ^- magnetic moment analysis because of the presence of a contaminating line of unknown origin in the $12 \rightarrow 11$ Σ^-U transition.[7]

A. Noncircular transitions

Simulated data were generated using values of G [see Eq. (10)] ranging from 0.0 to 0.25 with the width, total number of counts, and background rate taken from the set of K^--Σ^- data in Pb with the greatest number of K^- stops. For each set of simulated data, the computer random number generator was reset to the same initial value to ensure that the only variable among the different sets of data was the value of G. The results of this analysis of the simulated data showed that the value obtained for the magnetic moment is very sensitive to the contribution from the first noncircular transition.

Simulated data were also generated for several $\bar{p}$ transitions and the analysis showed the magnetic moment to be similarly sensitive to contributions from the first noncircular transition.

G was fitted as a free parameter in the analysis of the U-$\bar{p}(12 \rightarrow 11)$, U-$\bar{p}(11 \rightarrow 10)$, and Pb-$\bar{p}(11 \rightarrow 10)$ transitions. For the higher transitions, G was determined from the data, if the appropriate $\Delta n = -2$

transition was in the experimentally obtained spectrum, or from a cascade calculation otherwise.

The set of K^--Σ^- data representing the largest number of K^- stops was analyzed for the $\Sigma^-(12\rightarrow11)$ fine-structure splitting for two extreme values of G. These values were chosen for both the Σ^- and $\bar{p}$ data from the following considerations. Since the Σ^- atomic energy levels in Pb have approximately the same Bohr radii as the corresponding $\bar{p}$ levels in U, we chose a range of G which was consistent with the U-$\bar{p}(12\rightarrow11)$ analysis and with the upper limit obtained directly from the Σ^- data. We thus chose a range from 0.05 to 0.15 for G in the Pb Σ^- analysis. The results of the analysis for $G=0.05$ and $G=0.15$ for these data are shown in Fig. 6. The width of the region over which χ^2 changed by one unit was approximately the same for the two values of G, but the center was shifted. The region size was increased by 20% if one took the upper limit from the χ^2 curve for $G=0.15$ and the lower limit from the curve for $G=0.05$. Similarly, the range for G was chosen to be from 0.10 to 0.20 for Pt.

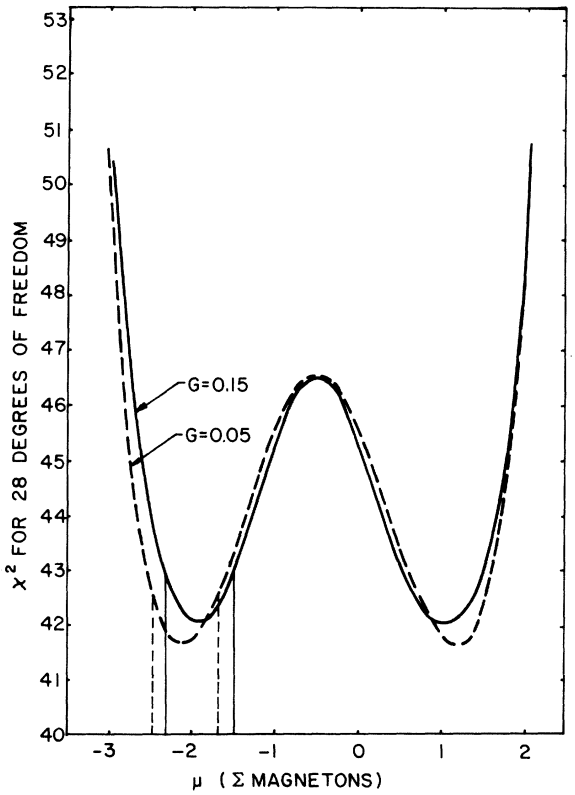

FIG. 6. χ^2 curves from fitting $\Sigma^-(12\rightarrow11)$ in natural Pb with two different values of G [Eq. (10)]. The region between the dashed vertical bars is the range over which χ^2 changes by 1 unit for the curve with $G=0.05$. The region between the solid vertical bars is the range over which χ^2 changes by 1 unit for the curve with $G=0.15$.

B. Uncertainties in instrumental width

When a single Gaussian such as a computer-simulated line or a radioactive source line in a calibration run was fitted to a doublet function with $R=1.096$ [the value from Eq. (4b) for a circular $(12\rightarrow11)$ transition] and a fixed instrumental width, the χ^2 function was centered about zero separation, but there was a finite interval over which χ^2 changed by one unit. This range was a reflection of statistical uncertainties in the width of the single Gaussian. Simulated data were generated with these single Gaussians for different amplitudes on the same background. As the amplitude was increased, the region over which χ^2 changed by one unit decreased, because of the improvement in the precision of the width with increasing signal-to-background.

Because a statistical error is associated with each instrumental width, it was necessary to carry out the doublet analysis on the $\bar{p}$ or Σ^- data for several widths and to include the effects of their uncertainties in the quoted errors. For sufficiently large separations between the doublet components such as were present for the Pb-$\bar{p}(12\rightarrow11)$ and $(11\rightarrow10)$ and the U-$\bar{p}(13\rightarrow12)$, $(12\rightarrow11)$, and $(11\rightarrow10)$ transitions, there was little sensitivity to the width used, and in fact, a change of five standard deviations in the instrumental width for the last two lines in U caused less than a 2% change in the extracted value of $\mu(\bar{p})$.

C. Statistical population of fine-structure levels

The fine-structure components of the $\bar{p}(11\rightarrow10)$ in U were separated by more than one FWHM so it was possible to make a free fit to all parameters including G of a doublet function plus an exponential background. The only constraint was that the two component lines have the same width. This fit provided a measurement of the ratio R [Eq. (8)]. The result was $R=1.27\pm0.19$ which was in agreement with 1.11, the value obtained using Eq. (4b). One can thus conclude that the statistical population of the fine-structure states is not significantly changed by, e.g., $M1$ Auger transitions, a result which agrees with the calculation discussed in Sec. II. The assumption that R (and R') could be held fixed and equal to the values obtained from Eq. (4a) appears justified.

D. Dependence of results on region of fit

The spectra obtained from $\bar{p}$ in Pb and U and K^- in Pt and ^{208}Pb are displayed in Figs. 7 through 10. In the $\bar{p}$ data the lines were well separated

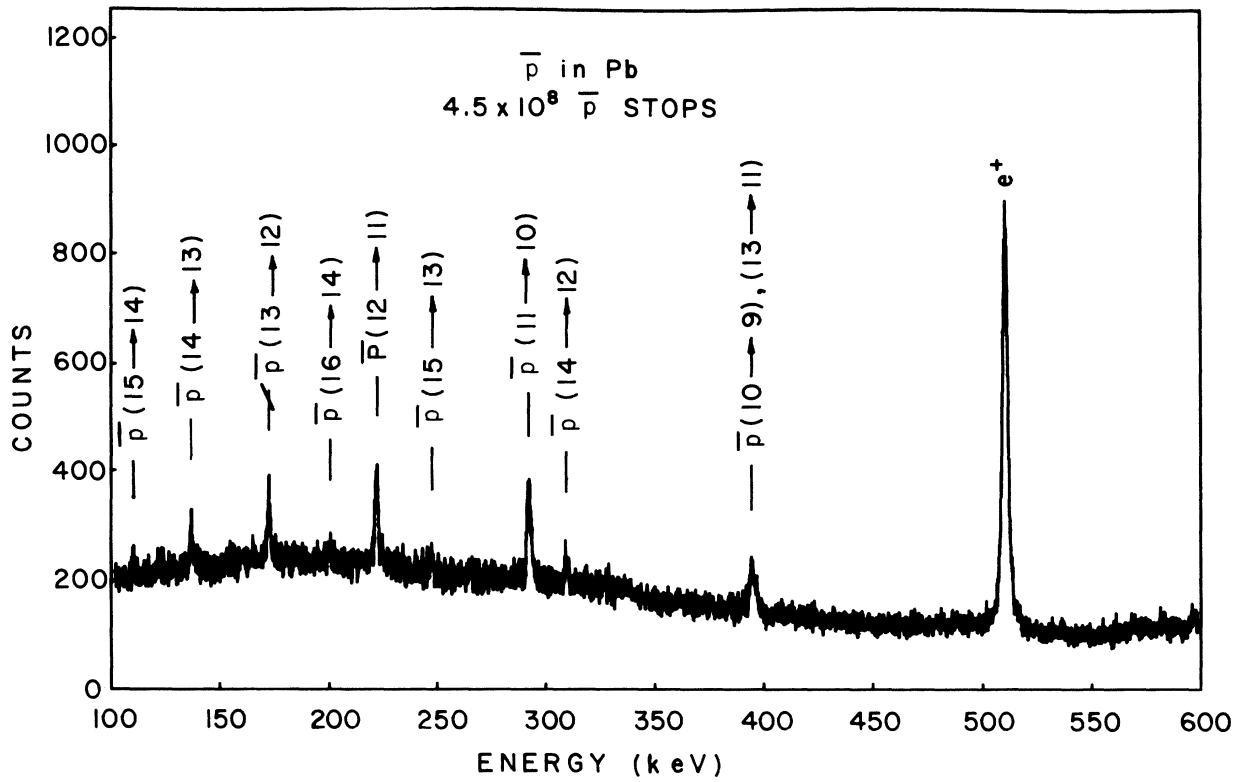

FIG. 7. x-ray spectrum obtained by stopping $\bar{p}$ in natural Pb. The data represent 4.5×10^8 $\bar{p}$ stops.

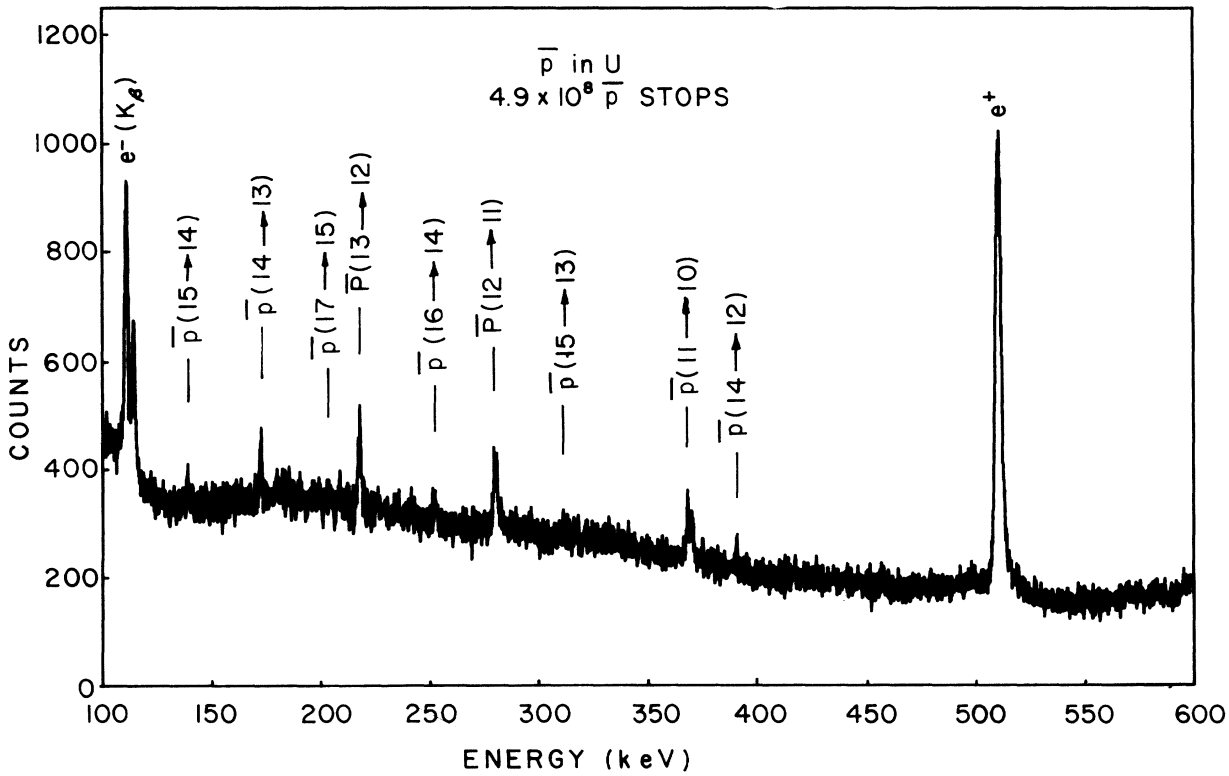

FIG. 8. x-ray spectrum obtained by stopping $\bar{p}$ in U. The data represent 4.9×10^8 $\bar{p}$ stops.

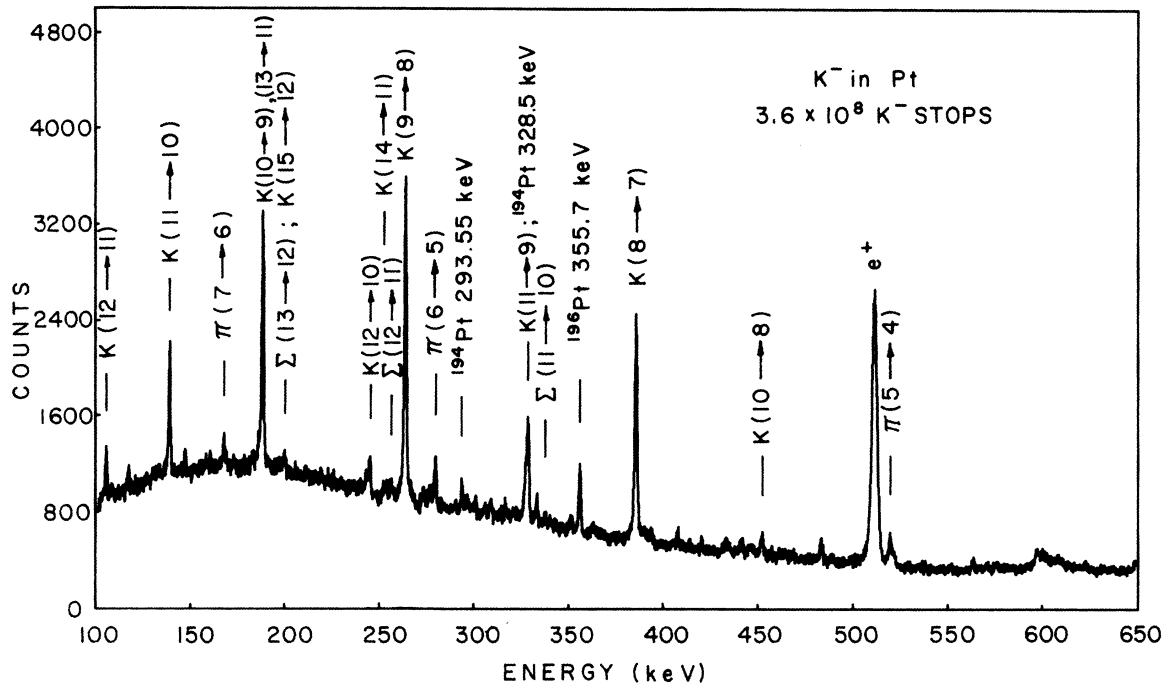

FIG. 9. x-ray spectrum obtained by stopping K^- in Pt. The data represent 3.6×10^8 K^- stops.

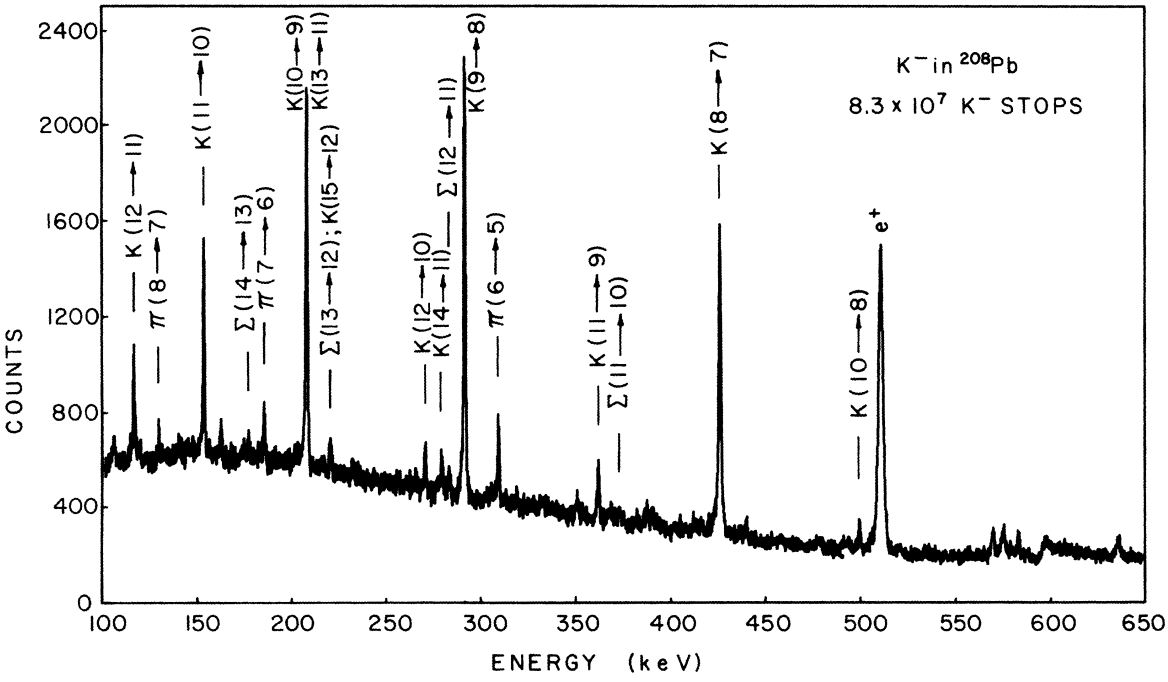

FIG. 10. x-ray spectrum obtained by stopping K^- in ^{208}Pb. The data represent 8.3×10^7 K^- stops.

and there was no difficulty selecting a range of energies so as to include an ample region of background on both sides of the relevant peak. Due to the close proximity of the $K^-(9 \rightarrow 8)$ and $K^-(14 \rightarrow 11)$ lines on the high- and low-energy sides respectively of the $\Sigma^-(12 \rightarrow 11)$ line, the dependence of the χ^2 function on the region over which the data were fitted was studied. Figure 11 shows a series of χ^2 functions generated by successively decreasing the region of fit by one channel on each side of the $\Sigma^-(12 \rightarrow 11)$ in ^{208}Pb (with $G=0$). Although there were slight fluctuations in the χ^2 function, it was not statistically significant. The other Σ^- data exhibited a similar independence of the region over which the fit was made.

E. The antiproton magnetic moment

The $\Delta n = -1$ $\bar{p}$ transitions from the levels $n = 13$, 12, and 11 in both Pb and U were analyzed for fine-structure splitting. The χ^2 function obtained for the $\bar{p}(11 \rightarrow 10)$ transition in U is shown in Fig. 12. One can observe that the sign of $\mu(\bar{p})$ is negative and that the two curves representing different instrumental widths almost coincide in the region of the minimum χ^2. The results of a free fit to the U-$\bar{p}(11 \rightarrow 10)$ transition are shown in Fig. 13. Table II is a compilation of the values obtained for $\mu(\bar{p})$ from analysis of the $\Delta n = -1$ transitions from $n = 13$, 12, and 11 in both U and Pb.

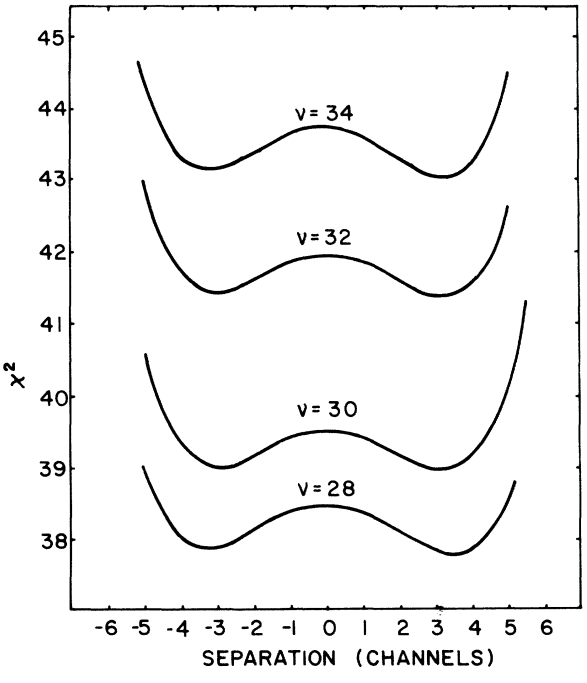

FIG. 11. χ^2 curves generated for several regions of fit for the $\Sigma^-(12 \rightarrow 11)$ transition in ^{208}Pb with $G=0$. Each successive curve was generated by decreasing the region by one channel (148 eV) on each side. The number of degrees of freedom is indicated by ν.

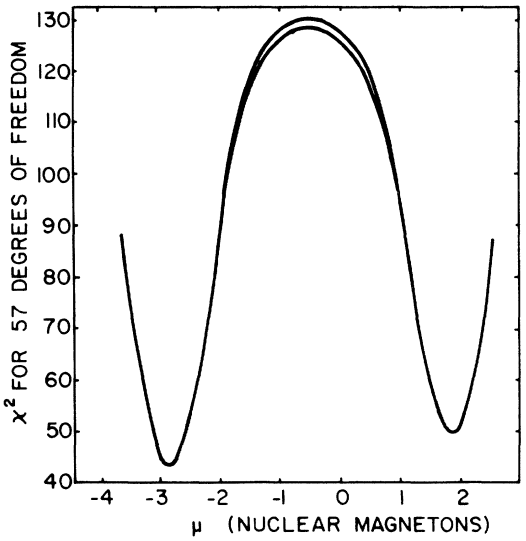

FIG. 12. χ^2 curves for the $\bar{p}(11 \rightarrow 10)$ transition in U. The χ^2 difference between the two minima is 6.7. The two curves plotted are for instrumental widths that are one standard deviation greater and one standard deviation less than the measured value.

One should note that the value for $\mu(\bar{p})$ derived from the Pb-$\bar{p}$ $(11 \rightarrow 10)$ transition, as listed in Table II, is substantially different from a value reported previously.[6] This discrepancy arises from a failure to include the contribution from the first noncircular transition in the earlier analysis of the data.

The weighted average of the values of $\mu(\bar{p})$ as shown in Table II is

$$\mu(\bar{p}) = (-2.819 \pm 0.056)\mu_N,$$

where μ_N is the nuclear magneton $e\hbar/2m_p c$. The error quoted is the root-mean-square error since

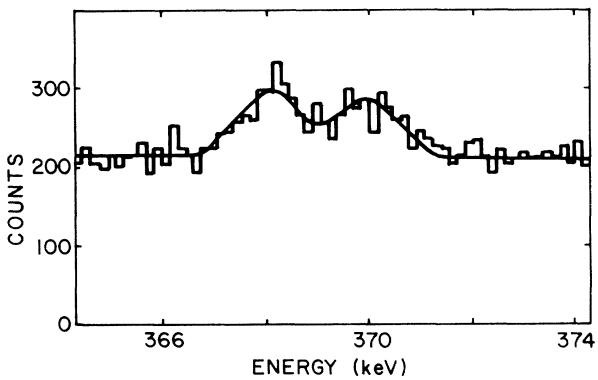

FIG. 13. $\bar{p}(11 \rightarrow 10)$ transition in U. The smooth curve represents a free fit to the data.

the six measurements of Table II represent a consistent set. This value is in good agreement with that of 2.793 μ_N for the proton and is opposite in sign. It is also in agreement with, but much more precise than, the earlier measurement of Button and Maglic,[36] who obtained $(-1.8\pm1.2)\ \mu_N$ from a double scattering experiment in a hydrogen bubble chamber.

F. The Σ^- magnetic moment

Each set of Σ^- data in Pt and Pb was analyzed for fine-structure splitting, and the individual curves of χ^2 vs Σ^- magnetic moment were added together to yield the result shown in Fig. 14. The χ^2 response for the total data represented in this figure was obtained with G fixed at 0.10 for the Pb data and at 0.15 for the Pt data. The range of $\mu(\Sigma^-)$ shown between the two vertical lines in this figure incorporates the error due to the instrumental width but not that due to the uncertainties in the contributions from noncircular transitions. This error was increased by 20% to include uncertainties in the contributions from the noncircular component in the $\Sigma^-(12\rightarrow11)$ transition.

From Fig. 14 one notes a statistical preference for a negative sign for the Σ^- magnetic moment, the χ^2 difference between the two minima being 0.95 for one χ^2 curve and 0.82 for the other. The final value obtained for $\mu(\Sigma^-)$ is

$$\mu(\Sigma^-)=(-1.89\pm0.47)\ \mu_\Sigma,$$

or equivalently

$$\mu(\Sigma^-)=(-1.48\pm0.37)\ \mu_N.$$

The value for $\mu(\Sigma^-)$ differs by 1.6 standard deviations from the SU(3) value of $-0.9\ \mu_N$. One should note, however, that, as predicted by SU(3), our result is in agreement with the recent measurement of $\mu(\Xi^-)$ by Cool *et al.*,[37,38] who obtained

$$\mu(\Xi^-)=(-2.1\pm0.8)\ \mu_N.$$

Since the mass of the Σ^- is 27% greater than that of the proton, the presence of an appreciable mass correction term in the magnetic moment would not be surprising. However, as mentioned by Cool *et al.*,[37,38] there is at present no fully acceptable method for calculating such a correction, and this is confirmed by a recent paper of Caldi and Pagels.[39] At the present level of experimental precision and theoretical understanding no definitive disagreement with the value predicted from Eq. (2) is implied by our result.

Note added in proof. Since submission of this paper, a Columbia-Yale group has reported[40] measurements of the $\bar{p}$ and Σ^- magnetic moments which are in substantial agreement with the values reported here.

TABLE II. Magnetic moment of the $\bar{p}$ derived from antiprotonic x rays in Pb and U. For all transitions shown, R was assumed to be the appropriate statistical ratio a/c given by Eq. (4b). The contribution G of the first noncircular transition was fitted as a free parameter in the data analysis for the $12\rightarrow11$ and $11\rightarrow10$ transitions in U and for the $11\rightarrow10$ transition in Pb.

Element	Transition	μ $(e\hbar/2m_pc)$
Pb	$13\rightarrow12$	-2.70 ± 0.85
	$12\rightarrow11$	-2.76 ± 0.55
	$11\rightarrow10$	-2.58 ± 0.21
U	$13\rightarrow12$	-2.78 ± 0.65
	$12\rightarrow11$	-2.81 ± 0.13
	$11\rightarrow10$	-2.847 ± 0.066
	weighted average	-2.819 ± 0.056

ACKNOWLEDGMENTS

We wish to express our appreciation to Dr. David Berley, Dr. Donald Lazarus, Dr. Y. Y.

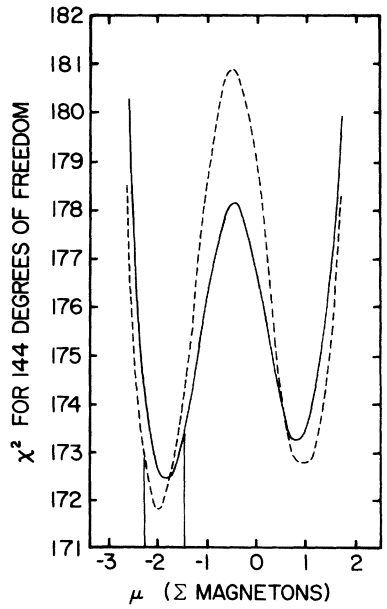

FIG. 14. χ^2 curves from fitting the $\Sigma^-(12\rightarrow11)$ transitions. The curves represent a compilation of data from natural Pb ($5.4\times10^8\ K^-$ stops), ^{208}Pb ($8.3\times10^7\ K^-$ stops), and Pt ($3.6\times10^8\ K^-$ stops). The solid curve was calculated for instrumental resolution that was one standard deviation greater than the most probable; the dotted curve for one standard deviation less. Included in the error for the Σ^- moment (see text) but not indicated in this figure is the uncertainty introduced by contributions from noncircular transitions.

Lee, Dr. R. H. Phillips, Dr. R. R. Rau, and the staff of the Brookhaven National Laboratory Alternating Gradient Synchrotron for their support, to Dr. Carl Carlson, Dr. John Delos, and Dr. Hans von Baeyer for helpful discussions on the Auger calculation, *CPT*, and SU(3) symmetries, and to Pat Hand for her untiring efforts in all aspects of the data analysis.

---

*Work supported in part by the National Science Foundation and the U. S. Atomic Energy Commission.

†The results presented here constitute part of a thesis submitted to the College of William and Mary in partial fulfillment of the requirements for the Ph.D. degree. Present address: Rutherford Laboratory, Chilton, Didcot, Oxon, England.

‡Present address: California Institute of Technology, Pasadena, California 91125.

§Present address: DESY, Hamburg, Germany.

[1]E. Fermi and E. Teller, Phys. Rev. 72, 399 (1947).

[2]M. Y. Au-Yang and M. L. Cohen, Phys. Rev. 174, 468 (1968).

[3]S. S. Gerstein, V. I. Petrukhin, L. I. Ponomarev, and Y. D. Prokoshkin, Usp. Fiz. Nauk. 97, 3 (1969) [Soviet Phys.—Usp. 12, 1 (1969)].

[4]A. H. de Borde, Proc. Phys. Soc. London Sect. A 67, 57 (1954).

[5]D. Zieminska, Phys. Lett. 37B, 403 (1971).

[6]J. D. Fox, P. D. Barnes, R. A. Eisenstein, W. C. Lam, J. Miller, R. B. Sutton, D. A. Jenkins, R. J. Powers, M. Eckhause, J. R. Kane, B. L. Roberts, M. E. Vislay, R. E. Welsh, and A. R. Kunselman, Phys. Rev. Lett. 29, 193 (1972).

[7]J. D. Fox, W. C. Lam, P. D. Barnes, R. A. Eisenstein, J. Miller, R. B. Sutton, D. A. Jenkins, M. Eckhause, J. R. Kane, B. L. Roberts, R. E. Welsh, and A. R. Kunselman, Phys. Rev. Lett. 31, 1084 (1973).

[8]B. L. Roberts, C. R. Cox, M. Eckhause, J. R. Kane, R. E. Welsh, D. A. Jenkins, W. C. Lam, P. D. Barnes, R. A. Eisenstein, J. Miller, R. B. Sutton, A. R. Kunselman, R. J. Powers, and J. D. Fox, Phys. Rev. Lett. 32, 1265 (1974).

[9]B. L. Roberts, C. R. Cox, M. Eckhause, J. R. Kane, R. E. Welsh, D. A. Jenkins, W. C. Lam, P. D. Barnes, R. A. Eisenstein, J. Miller, R. B. Sutton, A. R. Kunselman, R. J. Powers, and J. D. Fox, Phys. Rev. Lett. 33, 1181 (1974).

[10]See, for example, J. J. Sakurai, *Invariance Principles and Elementary Particles* (Princeton Univ. Press, Princeton, New Jersey, 1964), p. 148.

[11]See, for example, J. Bernstein, G. Feinberg, and T. D. Lee, Phys. Rev. 139, B1650 (1965).

[12]M. Nauenberg, Phys. Rev. 135, B1047 (1964).

[13]S. Coleman and S. L. Glashow, Phys. Rev. Lett. 6, 423 (1961).

[14]H. R. Rubinstein, F. Scheck, and R. H. Solocow, Phys. Rev. 154, 1608 (1967).

[15]For a discussion of magnetic moments and fine-structure splitting see H. A. Bethe and E. Salpeter, *Quantum Mechanics of One- and Two-Electron Atoms* (Academic, New York, 1957), starting with Sec. 10; also J. J. Sakurai, *Advanced Quantum Mechanics* (Addison-Wesley, Reading, Mass., 1967), Sec. 3-5.

[16]W. W. Sapp, Jr., College of William and Mary Report No. WM70-21, 1970 (unpublished); W. W. Sapp, Jr., M. Eckhause, G. H. Miller, and R. E. Welsh, Phys. Rev. C 5, 690 (1972).

[17]L. Wilets, K. Dan. Vidensk. Selsk. Mat.-Fys. Medd. 29, 3 (1954).

[18]B. A. Jacobsohn, Phys. Rev. 96, 1637 (1954).

[19]M. Y. Chen, Phys. Rev. C 1, 1176 (1970).

[20]G. Ara and M. Y. Chen, Bull. Am. Phys. Soc. 19, 599 (1974).

[21]S. C. Cheng, Y. Asano, M. Y. Chen, J. Dugan, E. Hu, L. Lidofsky, W. Patton, C. S. Wu, D. Lu, and V. Hughes, Bull. Am. Phys. Soc. 19, 599 (1974).

[22]R. J. McKee, Phys. Rev. 180, 1139 (1969).

[23]Y. Eisenberg and D. Kessler, Nuovo Cimento 19, 1195 (1961).

[24]G. R. Burbidge and A. H. de Borde, Phys. Rev. 89, 189 (1953).

[25]J. C. Slater, *Quantum Theory of Atomic Structure* (McGraw-Hill, New York, 1960), Vol. I, p. 368 ff.

[26]P. A. M. Dirac, Proc. R. Soc. London Ser. A 114, 243 (1927).

[27]J. D. Fox, BNL Accelerator Dept. EP & S Division Technical Note No. 7, 1967 (unpublished).

[28]J. D. Fox, BNL Accelerator Dept. EP & S Division Technical Note No. 20, 1968 (unpublished).

[29]M. Zeller, L. Rosenson, and R. E. Lanou, Jr., BNL AGS Summer Study, BNL Report No. BNL16000, 1970 (unpublished).

[30]A. S. Carroll, T. F. Kycia, K. K. Li, D. N. Michael, P. M. Mockett, D. C. Rahm, and R. Rubinstein, BNL Accelerator Dept. EP & S Division Technical Note No. 54, 1972 (unpublished).

[31]V. Fitch and R. Motley, Phys. Rev. 101, 496 (1956).

[32]J. T. Routti and S. G. Prussin, Nucl. Instrum. Methods 72, 125 (1969).

[33]See, for example, P. R. Bevington, *Data Reduction and Error Analysis for the Physical Sciences* (McGraw-Hill, New York, 1969).

[34]See A. Sommerfeld, *Optics* (Academic, New York, 1964), p. 289.

[35]Particle Data Group, Rev. Mod. Phys. 45, S16 (1973).

[36]J. Button and B. Maglic, Phys. Rev. 127, 1297 (1962).

[37]R. L. Cool, G. Giacomelli, E. W. Jenkins, T. F. Kycia, B. A. Leontic, K. K. Li, and J. Tieger, Phys. Rev. Lett. 29, 1630 (1972).

[38]R. L. Cool, G. Giacomelli, E. W. Jenkins, T. F. Kycia, B. A. Leontic, K. K. Li, and J. Tieger, Phys. Rev. D 10, 792 (1974).

[39]D. G. Caldi and Heinz Pagels, Phys. Rev. D 10, 3739 (1974).

[40]G. Dugan *et al.*, Bull. Am. Phys. Soc. 20, 701 (1975); E. Hu *et al.*, *ibid.* 20, 701 (1975).